Proceedings of the ASME 2020
International Design Engineering Technical Conferences
and Computers and Information in Engineering Conference
IDETC/CIE2020
August 17-19, 2020, Virtual, Online

DETC2020-22398

ON THE NONLINEAR MODE-COUPLING IN ULTRA PRECISION

MANUFACTURING MACHINES: EXPERIMENTAL AND ANALYTICAL ANALYSES

Sunit K. Gupta, Mohammad A. Bukhari, Oumar R. Barry*

Department of Mechanical Engineering
Virginia Tech
Blacksburg, Virginia 24061
Email: obarry@vt.edu

Chinedum E. Okwudire

Department of Mechanical Engineering
University of Michigan
Ann Arbor, Michigan 48105
Email: okwudire@umich.edu

ABSTRACT

Recent studies in passively-isolated systems have shown that mode coupling is desirable for best vibration suppression, thus refuting the long-standing rule of mode decoupling. However, these studies have ignored the nonlinearities in the isolators. In this work, we consider stiffness nonlinearity from pneumatic isolators and study the nonlinear free undamped vibrations of a passively-isolated ultra-precision manufacturing (UPM) machine. Experimental analysis is conducted to guide the mathematical formulation. The system comprises linearly and nonlinearly coupled in-plane horizontal and rotational motion of the UPM machine with quadratic nonlinear stiffness from the isolators. We present closed-form expressions using the method of multiple scales for two cases viz. the nonresonant case and the bounded internal resonance case. We validate our theoretical findings through direct numerical simulations. For the non-resonant case, we show that the system behaves similar to a linear system. However, for the nearly internal resonance case, we demonstrate strong energy exchange between the modes stemming from nonlinear mode coupling. We further study the effect of nonlinear mode coupling on the vibration isolation performance and demonstrate that mode coupling is not always desirable.

INTRODUCTION

Over the last few years, use of machine parts with micro-level patterns and nano-level surface finish has significantly increased in the electronic, biomedical, and communication industries [1–3]. To meet the stringent

requirements at the micro-scale, ultra-precision manufacturing (UPM) machines like ultra precision machine tools, water steppers, and micro coordinate measuring machine (CMM) are used to manufacture these parts. As the tolerance and accuracy of these parts are very high, even the smallest amplitude of vibrations can adversely affect the accuracy and precision of the UPM machine. Vibration isolation of UPM machines can be achieved

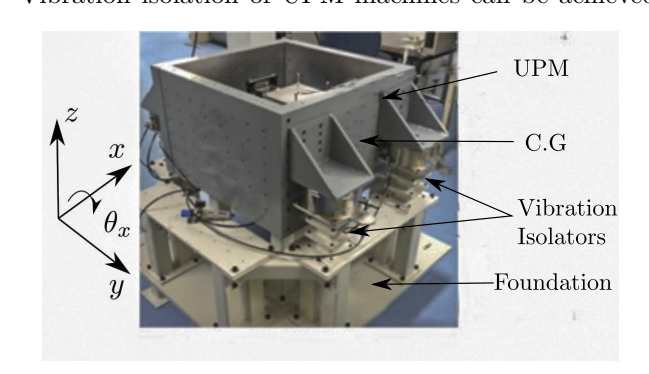
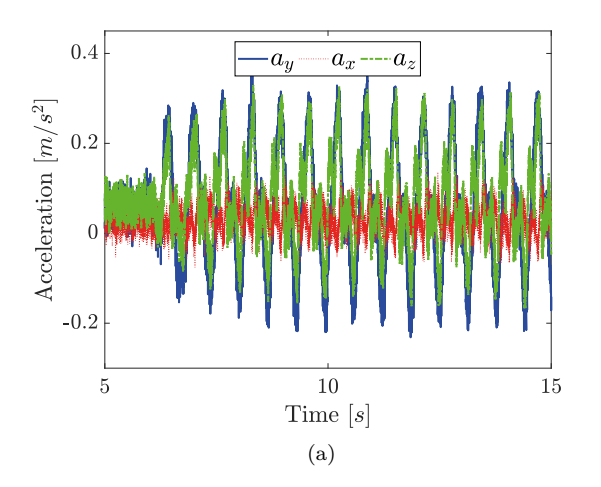


FIGURE 1: Experimental setup

by passive, active, or semi-active isolators [4–6]. However, passive isolators have been found more useful as compared to active and semi-active because of the their cost effectiveness, reliability and simple installation [7–9]. Good passive isolation from the surrounding vibrations can be achieved when the stiffness of the isolator is very low. However, low stiffness causes the residual vibrations in the form of low frequency rocking motions due to internal or external excitation [10]. These residual vibrations must be minimized because they can damage the accuracy of the machine [7, 8, 11, 12]. Another drawback of passive isolators is the increased transmissibility at fre-

^{*}Address all correspondence to this author.



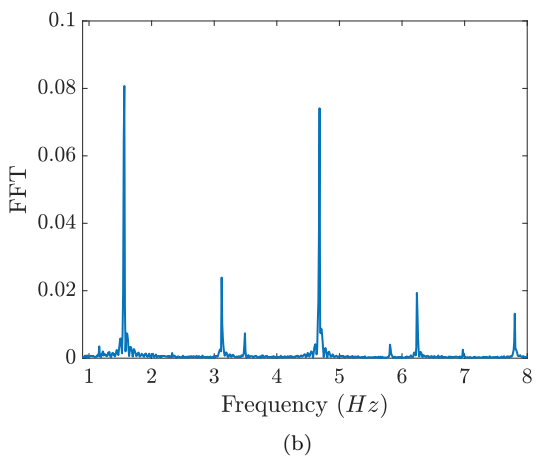


FIGURE 2: Experimental Results Showing (a) Time Response; (b) Natural Frequencies

quencies greater than resonance with viscous damped oscillator [6, 7, 11]. These two drawbacks can be avoided using pneumatic isolators (i.e. nonlinear vibration isolators) [10, 13-18].

A critical factor in designing these pneumatic isolators is the selection of the isolator location such that mode coupling can be avoided [8]. The decoupling between the modes can be achieved by aligning the isolator mounting with the center of gravity of the UPM machine [11,19,20]. This decoupling of modes restricts the transmission of vertical ground motion to the horizontal axis and further prevents the rocking motion of the UPM machine [8,12]. Also, this decoupling avoids the presence of other peaks in the transmissibility response of the machine [21]. However, the proper selection of the isolator mounting points is often ignored in the design phase [7,8].

A mathematical model to represent linear mode coupling in UPM machine was first developed by Okwudire [13,22]. It was shown that residual vibrations and transmissibility can be reduced by selecting the proper isolator location, motor, and work surface heights. Also, it was demonstrated that mode coupling is desirable to minimize the residual vibration and accordingly they obtained the optimum value of the location of passive isolator from the center of gravity of UPM [13]. It was observed that with this optimum location of isolator, fivefold reduction in the vibration amplitude can be achieved. This observation is in contrary to the earlier observations of aligning the isolator with the center of gravity of UPM to avoid mode coupling and consequently to reduce the transmitted vibration.

However, in Okwudire's work [13, 22], the nonlinear stiffness of the pneumatic isolators was not considered and accordingly its effect on the location of the isolators was not explored. The aim of this work is to investigate whether the benefits demonstrated in linear mode coupling can be extended to nonlinear mode coupling. Towards realizing this aim, here we consider the nonlin-

earity in the stiffness of the pneumatic isolators and study the nonlinear dynamic of the passively-isolated UPM machine. Experiments are carried out to guide the mathematical formulation. The exact coupled nonlinear equations of motion of the isolated machine are presented, and the analytical solutions are obtained using the method of multiple scales. Direct numerical simulations are used to validate the analytical results. Parametric studies are performed to understand how nonlinear mode coupling affects the performance of the pneumatic isolators.

Experimental results

Experiments are carried out using the reconfigurable UPM machine based prototype depicted in Fig. 1. The prototype consists of an 800 kg base of dimensions 749.3x749.3x495.3 mm. The machine is supported by four pneumatic isolators (Bilz model BiAir 1-ED). The UPM machine is disturbed with initial displacements in the y-direction and the vibration of the system is measured using a tri-axial accelerometer (PCB Piezotronics model Y356A63) with the sensitivity of 10.58 mV/g. The experimental results show that the prototype machine can exhibit either stable or unstable motion depending on the applied initial displacement. A very low initial disturbance yields a stable vibration motion while a relatively larger displacement exhibits an unstable motion. Figure 2a shows the experimental time response of the vibrating UPM machine in all three directions. The instability can be observed in all directions; however, higher vibration amplitudes occur in the v and zdirections. This is expected as the system is disturbed in the y-direction, resulting in coupling in the y-z plane. A plot of the Fast Fourier Transform of the previously discussed time response graph is shown in Fig. 2b. The frequencies corresponding to the peaks in this plot are the first six linear and nonlinear modes of the UPM machines in 3D and are 1.56, 3.12, 3.5, 4.68, 6.24, 7.792 Hz. Note that the fundamental frequency of the UPM is nearly half of the second mode, which corresponds to subharmonic resonance. This observation suggests that the stiffness of the pneumatic isolator is of a quadratic nonlinear type, thus confirming the type of nonlinearity of the pneumatic isolator mentioned in the literature [23].

MATHEMATICAL FORMULATION

In this section, we outline the mathematical model for the UPM, followed by the linear and nonlinear analyses. Note that the linear analysis of vibrations of UPM machines is already established in the literature. However, the nonlinear analysis of these vibrations is not fully resolved yet. For this purpose, we use one of the perturbation methods viz. method of multiple scales and obtain the closed-form solutions of the amplitude of vibrations.

Mathematical Model

A schematic of the 2D model of an isolated UPM has been shown in Fig. 3. In this figure, m and I represent the mass and centroid moment of inertia of the UPM about the y-axis, respectively. k_y and k_z are the combined linear stiffness of the isolators in y and z-directions, respectively, q_y and q_z are the quadratic nonlinear stiffness of the isolators in y and z-directions, respectively, and b and b are the distance of the isolators from the centroid (C.G.) in the horizontal and vertical directions, respectively.

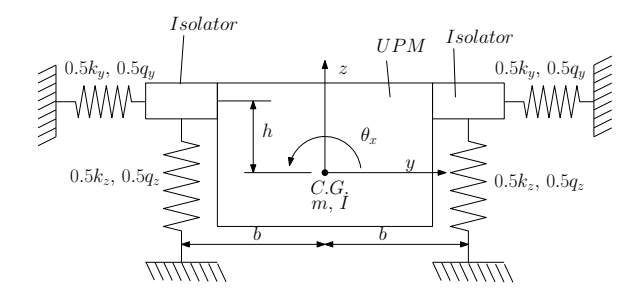


FIGURE 3: Schematic of UPM with isolators with quadratic nonlinearity

It should be noted that the current work only focuses on the y-z plane motions. This assumption further implies that we are considering 2-degree of freedom for the current system viz. horizontal and rotational motion (y and θ_x motion). Hence, if there is no damping in the system the equations of motion for the UPM can be written as

$$m\ddot{y} + k_y(y - h\sin(\theta_x)) + q_y(y - h\sin(\theta_x))^2 = 0, \quad (1a)$$

$$I\ddot{\theta}_x + k_z b(b\sin(\theta_x)) + q_z b(b\sin(\theta_x))^2$$
(1b)

$$-k_y h(y - h\sin(\theta_x)) - q_y h(y - h\sin(\theta_x))^2 = 0.$$

For small amplitude motion the above equation can be rewritten as

$$m\ddot{y} + k_y(y - h\theta_x) + q_y(y - h\theta_x)^2 = 0, \qquad (2a)$$

$$I\ddot{\theta}_x + k_\theta \theta_x + q_\theta \theta_x^2 - q_y h(y - h\theta_x)^2 - k_y h(y - h\theta_x) = 0.$$
(2b)

where $k_{\theta} = b^2 k_z$ and $q_{\theta} = b^3 q_z$. The above equations describe the evolution of the two coupled modes with time. The nonlinear analysis of the system is presented in the next section.

Analysis

Our first interest in this work is to understand the effect of h on the different modes of vibration in the UPM machine. For this purpose we use the method of multiple scales (MMS). We focus on small amplitude oscillations by introducing a small parameter ϵ (i,e,. $\epsilon \ll 1$) in the governing equations of motion through rescaling

$$y(t) = y_s + \epsilon \eta(t) \tag{3a}$$

$$\theta_x(t) = \theta_{xs} + \epsilon \vartheta(t) \tag{3b}$$

where y_s and θ_{xs} are the equilibrium steady states of the system and $\eta(t)$ and $\vartheta(t)$ are the small perturbations around y_s and θ_{xs} , respectively. Since we are considering the free undamped vibration of UPM, the steady states y_s and θ_{xs} will be zero. Accordingly, substitution of the above rescaling in the equations of motion (Eq.2) leads

$$m\ddot{\eta} + k_y(\eta - h\vartheta) + \epsilon q_y(\eta - h\vartheta)^2 = 0, \qquad (4a)$$

$$I\ddot{\vartheta} + k_{\theta}\vartheta - k_{y}h(\eta - h\vartheta) + \epsilon q_{\theta}\vartheta^{2}$$

$$-\epsilon q_{y}h(\eta - h\vartheta)^{2} = 0.$$
(4b)

Note that we have divided the equation after substitution of re-scaling throughout ϵ to get the above equations. Since the nonlinear terms appears at $\mathcal{O}(\epsilon)$, the system becomes weakly nonlinear system. Before proceeding further, we need the solution of the linear unperturbed equation to build up the solution for the perturbed nonlinear equation. This is presented in the next section.

Linear Analysis In this section, linear analysis of the system given by Eq. (4) is presented. Note that, it is an important step to build up the solution for the perturbed nonlinear equation. The linearized coupled system can be obtained by setting $\epsilon=0$ in Eq. (4) and will be

$$m\ddot{\eta} + k_{\nu}(\eta - h\vartheta) = 0, \tag{5a}$$

$$I\ddot{\vartheta} + k_{\theta}\vartheta - k_{\upsilon}h(\eta - h\vartheta) = 0. \tag{5b}$$

To obtain the characteristic equation, we set $\eta(t) = \eta_0 \exp(\lambda t)$ and $\vartheta(t) = \vartheta_0 \exp(\lambda t)$ in Eq. 5 and obtain

$$m\lambda^2 \eta_0 + k_y(\eta_0 - h\vartheta_0) = 0, \tag{6a}$$

$$I\lambda^2\vartheta_0 + k_\theta\vartheta_0 - k_\eta h(\eta_0 - h\vartheta_0) = 0.$$
 (6b)

For the nontrivial solutions of the η_0 and ϑ_0 , the determinant of the coefficient matrix of the above equation must vanish. This solvability condition leads to

$$k_y I \lambda^2 + k_y k_\theta + m\lambda^4 I + m\lambda^2 k_\theta + m\lambda^2 k_y h^2 = 0.$$
 (7)

In order to obtain the natural frequency of the system we set $\lambda=i\omega$ in Eq. (7) and solve for ω . On solving the resultant equation for ω , we get the natural frequency of the system as $\omega_1=\sqrt{\frac{A+B}{2mI}}$, $\omega_2=\sqrt{\frac{A-B}{2mI}}$, where $A=mk_\theta+mk_yh^2+k_yI$ and $B=\sqrt{A^2-4mIk_yk_\theta}$. Accordingly, the solution of the linearized equation can be expressed as

$$\mathbf{y}(\tau) = A_1 \mathbf{r_1} e^{i\omega_1 t} + A_2 \mathbf{r_2} e^{i\omega_2 t} + C.C, \tag{8}$$

where $\mathbf{y}(\tau) = [\eta(\tau), \vartheta(\tau)]^T$, A_1 , A_2 are arbitrary constants and $\mathbf{r_1}$, $\mathbf{r_2}$ are the generalized right eigenvectors corresponding to the eigenvalues $\lambda = i\omega_1$ and $\lambda = i\omega_2$, respectively. For our system, $\mathbf{r_1}$ and $\mathbf{r_2}$ are

$$\mathbf{r_1} = \begin{bmatrix} \Lambda_1 \\ 1 \end{bmatrix}, \quad \mathbf{r_1} = \begin{bmatrix} \Lambda_2 \\ 1 \end{bmatrix} \tag{9}$$

with $\Lambda_i = \frac{k_y h}{k_y - m\omega_i^2}$. In our subsequent analysis, we need the generalized left eigen vectors corresponding to eigen values $\lambda = i\omega_1$ and $\lambda = i\omega_2$.

$$\mathbf{L_1} = \begin{bmatrix} l_1 & 1 \end{bmatrix}, \quad \mathbf{L_2} = \begin{bmatrix} l_2 & 1 \end{bmatrix}. \tag{10}$$

Since the coefficient matrix of the linear system of equation is symmetric in nature, l_1 and l_2 are the same as Λ_1 and Λ_2 i.e., $l_i = \frac{k_y h}{k_y - m \omega_i^2}$. These left eigenvectors play a crucial role in the removal of the secular terms in the nonlinear analysis which is presented next.

Nonlinear Analysis Using the Method of Multiple Scales. We note that the evolution of modulately large perturbation depends on the nature of nonlinearity present in the system. For the nonlinear analysis of Eq. (5), we have used the method of multiple scales (MMS) in the current work. To apply MMS, we first start with defining the multiple time scales as

$$T_0 = t, \quad T_1 = \epsilon t \tag{11}$$

with T_0 and T_1 are the fast and the slow time scales, respectively. With these time scales, the derivative operator gets perturbed to

$$\frac{\mathrm{d}}{\mathrm{d}t} = D_0 + \epsilon D_1 \,, \tag{12}$$

$$\frac{\mathrm{d}^2}{\mathrm{d}t^2} = D_{0,0} + 2\epsilon D_{0,1} \,, \tag{13}$$

where $D_n = \frac{\partial}{\partial T_n}$ and $D_{m,n} = \frac{\partial^2}{\partial T_m \partial T_n}$. Following the perturbation approach, the solution of perturbed nonlinear equation can be expressed as a series in powers of ϵ till $\mathcal{O}(\epsilon)$ as

$$\mathbf{y}(\tau) = \mathbf{y_0}(T_0, T_1) + \epsilon \mathbf{y_1}(T_0, T_1) = \mathbf{y_0} + \epsilon \mathbf{y_1},$$
 (14)

with $\mathbf{y}(\tau) = [\eta(t), \vartheta(t)]^T$, $\mathbf{y}_m = \mathbf{y_m}(T_0, T_1)$. On substitution of the above perturbed solution in Eq. (4) followed by a series expansion and equating the coefficient of similar power of ϵ to zero, we obtain the following coupled ODEs at different orders: $\mathcal{O}(\epsilon^0)$:

 $m\ddot{\eta_0} + k_y(\eta_0 - h\vartheta_0) = 0, \qquad (15a)$

$$I\ddot{\vartheta}_0 + k_\theta \vartheta_0 - k_\eta h(\eta_0 - h\vartheta_0) = 0. \tag{15b}$$

 $\mathcal{O}(\epsilon)$:

$$m\ddot{\eta}_1 + k_y(\eta_1 - h\vartheta_1) = 2q_y h\eta_0\vartheta_0 - 2mD_{1,0}\eta_0 - q_y h^2\vartheta_0^2 - q_y \eta_0^2$$
(16a)

$$I\ddot{\vartheta}_1 + k_\theta \vartheta_1 - k_y h(\eta_1 - h\vartheta_1) = -2q_y h^2 \eta_0 \vartheta_0 - q_\theta \vartheta_0^2 - 2ID_{1,0}\vartheta_0 + q_y h^3 \vartheta^2 + q_y h\vartheta_0^2$$
(16b)

The equations at $\mathcal{O}(\epsilon^0)$ are identical to the linearized equations (Eq. (5)). Accordingly, the solution of Eq. (15) can be written in the form of

$$\mathbf{y}(T_0, T_1) = A_1(T_1)\mathbf{r}_1 e^{i\omega_1 T_0} + A_2(T_1)\mathbf{r}_2 e^{i\omega_2 T_0} + C.C.$$
(17)

Note that A_1 and A_2 instead of being constants are now complex valued functions of slow time T_1 . On substituting the assumed solution for the $\mathbf{y_0}$ in the $\mathcal{O}(\epsilon)$ equations we get

$$m\ddot{\eta}_{1} + k_{y}(\eta_{1} - h\vartheta_{1}) = -A_{1}^{2}q_{y}(h - \Lambda_{1})^{2}e^{2i\omega_{1}T_{0}}$$

$$-A_{2}^{2}q_{y}(h - \Lambda_{2})^{2}e^{2i\omega_{2}T_{0}} - 2im\omega_{1}\Lambda_{1}D_{1}A_{1}e^{i\omega_{1}T_{0}}$$

$$-2im\omega_{2}\Lambda_{2}D_{1}A_{2}e^{i\omega_{2}T_{0}}$$

$$-2A_{1}\bar{A}_{2}q_{y}(h - \Lambda_{1})(h - \bar{\Lambda}_{2})e^{i(\omega_{1} - \omega_{2})T_{0}}$$

$$-2A_{1}A_{2}q_{y}(h - \Lambda_{1})(h - \Lambda_{2})e^{i(\omega_{1} + \omega_{2})T_{0}}$$

$$-2A_{1}\bar{A}_{1}(q_{\theta} + q_{y}h^{2}\Lambda_{1} + q_{y}h^{2}\bar{\Lambda}_{1} - 2q_{y}h\Lambda_{1}\bar{\Lambda}_{1}$$

$$-2q_{y}h^{3}) - 2A_{2}\bar{A}_{2}(q_{\theta} + q_{y}h^{2}\Lambda_{2} + q_{y}h^{2}\bar{\Lambda}_{2}$$

$$-2q_{y}h\Lambda_{2}\bar{\Lambda}_{2} - 2q_{y}h^{3}) + C.C \quad (18)$$

$$\begin{split} I\ddot{\vartheta}_{1} + k_{\theta}\vartheta_{1} - k_{y}h(\eta_{1} - h\vartheta_{1}) &= -A_{1}^{2}(q_{\theta} + 2q_{y}h^{2}\Lambda_{1} \\ - q_{y}h^{3} - q_{y}h\Lambda_{1}^{2})e^{2i\omega_{1}T_{0}} - A_{2}^{2}(q_{\theta} + 2q_{y}h^{2}\Lambda_{2} - q_{y}h^{3} \\ - q_{y}h\Lambda_{2}^{2})e^{2i\omega_{2}T_{0}} - 2iI\omega_{1}D_{1}A_{1}e^{i\omega_{1}T_{0}} \\ - 2iI\omega_{2}D_{1}A_{2}e^{i\omega_{2}T_{0}} - 2A_{1}\bar{A}_{2}(q_{\theta} + q_{y}h^{2}\Lambda_{1} \\ + q_{y}h^{2}\bar{\Lambda}_{2} - q_{y}h^{3} - q_{y}h\Lambda_{1}\bar{\Lambda}_{2})e^{i(\omega_{1} - \omega_{2})T_{0}} \\ - 2A_{1}A_{2}(q_{\theta} + q_{y}h^{2}\Lambda_{1} + q_{y}h^{2}\Lambda_{2} - q_{y}h^{3} \\ - q_{y}h\Lambda_{1}\Lambda_{2})e^{i(\omega_{1} + \omega_{2})T_{0}} - 2A_{1}\bar{A}_{1}(q_{\theta} + q_{y}h^{2}\Lambda_{1} \\ + q_{y}h^{2}\bar{\Lambda}_{1} - 2q_{y}h\Lambda_{1}\bar{\Lambda}_{1} - 2q_{y}h^{3}) \\ - 2A_{2}\bar{A}_{2}(q_{\theta} + q_{y}h^{2}\Lambda_{2} + q_{y}h^{2}\bar{\Lambda}_{2} - 2q_{y}h\Lambda_{2}\bar{\Lambda}_{2} \\ - 2q_{y}h^{3}) + C.C \quad (19) \end{split}$$

Note that substitution of y_0 in Eq. (16) leads to the appearance of resonant forcing terms $e^{i\omega_1 T_0}$, $e^{i\omega_2 T_0}$ and

their complex conjugate which further causes the unbounded growth in the solutions of the system. These terms causing the unbounded growth in the solution are known as secular terms and removal of these terms is necessary to get bounded solutions. Removal of these secular terms in the coupled ODE's requires the dot product of coefficient vectors of $e^{i\omega_1 T_0}$ and $e^{i\omega_2 T_0}$ to be zero [24]. But before proceeding further we present two situations in the system viz. nonresonant case and internal resonance case [25].

Non-Resonant Case In this case the natural frequencies of the system i.e., ω_1 and ω_2 are not commensurate. Then, for the bounded solution of $\mathbf{y_1}$, the solvability condition leads to

$$\mathbf{l_1} \cdot \mathbf{u_1} = 0 \quad \text{and} \quad \mathbf{l_2} \cdot \mathbf{u_2} = 0.$$
 (20)

where $\mathbf{u_1}$ and $\mathbf{u_2}$ are the coefficient vectors for $e^{i\omega_1 T_0}$ and $e^{i\omega_2 T_0}$, respectively. This solvability condition further leads to

 $D_1 A_n = 0 \Longrightarrow A_n = a_n e^{i\varpi_n}$ for n = 1 and 2 (21) where a_n and ϖ_n are constants and nonlinear frequency becomes equal to linear frequency.

Resonant Case In this case, the natural frequencies are proportionate or nearly commensurate. Accordingly, we can introduce a detuning parameter σ in system as

$$\omega_1 = 2\omega_2 + \epsilon\sigma \tag{22}$$

or
$$(\omega_1 - \omega_2)T_0 = (\omega_2 + \epsilon \sigma)T_0 = \omega_1 T_0 + \sigma T_1,$$
$$2\omega_2 T_0 = (\omega_1 - \epsilon \sigma)T_0 = \omega_2 T_0 + \sigma T_1.$$

On substituting above transformation in Eqs. (18) and (19) and removing the secular terms as discussed above we get

$$R_{2n} = -l_n R_{1n} \tag{23}$$

where

$$R_{11} = -2im\omega_1 \Lambda_1 D_1 A_1 - A_2^2 q_y (h - \Lambda_2)^2 e^{-i\sigma T_1}$$
 (24)

$$R_{21} = -2iI\omega_1 D_1 A_1 \tag{25}$$

$$-A_2^2(q_{\theta} - q_y h^3 - q_y h \Lambda_2^2 + 2q_y h^2 \Lambda_2) e^{-i\sigma T_1}$$

$$R_{12} = -2im\omega_2 \Lambda_2 D_1 A_2 \tag{26}$$

$$-2A_1\bar{A}_2q_y(h-\Lambda_1)(h-\Lambda_2)e^{i\sigma T_1}$$

$$R_{22} = -2iI\omega_2 D_1 A_2 - 2A_1 \bar{A}_2 (q_y - q_y h^3 + q_y h^2 \Lambda_1$$
 (27)
- $q_y h \Lambda_1 \bar{\Lambda}_2 + q_y h^2 \bar{\Lambda}_2) e^{i\sigma T_1}$.

As it is convenient to put up a polar notation, we express

$$A_n = \frac{a_n(T_1)}{2} e^{i\beta(T_1)}$$
 for $n = 1$ and 2 (28)

and consequently the complex conjugate of A_n , i.e.,

$$\bar{A}_n = \frac{a_n(T_1)}{2} e^{-i\beta(T_1)}$$
 for $n = 1$ and 2 (29)

Note that a_n and β_n are the real function of T_1 instead of being constants unlike the nonresonant case. Substituting these transformation in Eq. (23) and separating real and imaginary parts and solving for D_1a_n and $D_1\beta_n$ for n=1,2 we get the slow flow equations as

$$D_1 \beta_1 = \frac{a_2^2}{a_1} \Gamma_1 \cos(\gamma) \tag{30}$$

$$D_1 a_1 = a_2^2 \Gamma_1 \sin(\gamma) \tag{31}$$

$$D_1 \beta_2 = a_1 \Gamma_2 \cos(\gamma) \tag{32}$$

$$D_1 a_2 = -a_1 a_2 \Gamma_2 \sin(\gamma). \tag{33}$$

where Γ_1 , Γ_2 and γ are defined as

$$\Gamma_{1} = -\frac{1}{4} \frac{2l_{1}q_{y}h\Lambda_{2} + q_{y}h^{3} - q_{\theta} - l_{1}q_{y}h^{2} - l_{1}q_{y}\Lambda_{2}^{2}}{(l_{1}m\Lambda_{1} + I)\omega_{1}} - \frac{1}{4} \frac{-2q_{y}h^{2}\Lambda_{2} + q_{y}h\Lambda_{2}^{2}}{(l_{1}m\Lambda_{1} + I)\omega_{1}}$$
(34)

$$\Gamma_{2} = -\frac{1}{2} \frac{l_{2} q_{y} h \Lambda_{1} - l_{2} q_{y} h^{2} - l_{2} q_{y} \Lambda_{1} \bar{\Lambda}_{2} + l_{2} q_{y} h \bar{\Lambda}_{2}}{\omega_{2} (I + l_{2} m \Lambda_{2})} - \frac{1}{2} \frac{-q_{y} h^{2} \bar{\Lambda}_{2} - q_{\theta} + q_{y} h \Lambda_{1} \bar{\Lambda}_{2} - q_{y} h^{2} \Lambda_{1} + q_{y} h^{3}}{\omega_{2} (I + l_{2} m \Lambda_{2})}$$
(35)

and

$$\gamma = \beta_1 - 2\beta_2 + \sigma T_1 \tag{36}$$

The exact solution of the above differential equation can be expressed in terms of elliptic functions. Dividing Eq. (31) to (33) we get

$$\nu a_1 a_1' + a_2 a_2' = 0 \tag{37}$$

where $\nu = \frac{\Gamma_2}{\Gamma_1}$. On integrating the above equation we get

$$\nu a_1^2 + a_2^2 = E \tag{38}$$

where E is the constant of integration proportional to the initial energy in the system. From the above equation, we can observe that a_1 and a_2 will have the bounded solution if ν is positive i.e., Γ_1 and Γ_2 will always have the same sign. Differentiating Eq. (36) with respect to T_1 and changing the independent variable from T_1 to a_1 using Eqs (30),(32) and (38) we get

$$a_1 a_2^2 \cos(\gamma) + \frac{\sigma a_1^2}{2\Gamma_1} = L$$
 (39)

where L is the constant of integration. To get the single equation for a_2 , we assume $a_2^2 = E\xi$ which leads to $a_1^2 = \frac{E(1-\xi)}{\nu}$. Using Eq. (33) to remove γ from Eq. (39) and expressing a_1^2 and a_2^2 in terms of ξ , we obtain

$$\frac{\nu}{4E\Gamma_2^2} \left(\frac{d\xi}{dT_1}\right)^2 = (1-\xi)\xi^2
-\frac{\nu}{E^3} \left[L - \frac{\sigma E(1-\xi)}{2\nu\Gamma_1}\right]^2 = F^2(\xi) - G^2(\xi),$$
(40)

where
$$F = \pm \xi \sqrt{1 - \xi}$$
, $G = \pm \frac{\nu}{E^3}^{\frac{1}{2}} \left[L - \frac{\sigma E(1 - \xi)}{2\nu \Gamma_1} \right]$.

Note that for the real motion, $F^2 \ge G^2$. These points can be found by determining the fixed points (ξ_1, ξ_2, ξ_3)

of the right side of Eq. (40). If $\xi_1 \leq \xi_2 \leq \xi_3$, then the ξ is periodic between ξ_2 and ξ_3 but the motion is not. Based on this, ξ can be defined in terms of Jacobi elliptic function. Therefore, we use the following transformation

$$\frac{\nu}{4E\Gamma_2^2} \left(\frac{d\xi}{dT_1} \right)^2 = (\xi_3 - \xi)(\xi - \xi_2)(\xi - \xi_1). \tag{41}$$

Introducing the transformation

$$\xi_3 - \xi = \begin{cases} (\xi_3 - \xi_2) \sin^2(\chi), & \text{if } \sigma > 0\\ (\xi_3 - \xi_2) \cos^2(\chi), & \text{if } \sigma \le 0 \end{cases}$$
 (42)

in Eq. (41) and integrating we get

$$\xi = \begin{cases} \xi_3 - (\xi_3 - \xi_2) s n^2 [\kappa T_1, \zeta], & \text{if } \sigma > 0\\ \xi_3 - (\xi_3 - \xi_2) c n^2 [\kappa T_1, \zeta], & \text{if } \sigma \le 0 \end{cases}$$
(43)

where sn and cn are Jacobi elliptic function and $\kappa = \Gamma_1 \sqrt{\frac{E(\xi_3 - \xi_1)}{\nu}}$ and $\zeta = \sqrt{\frac{\xi_3 - \xi_2}{\xi_3 - \xi_1}}$. Using the definition of a_1^2 and a_2^2 we get the analogical solution in the form of

$$a_{1} = \begin{cases} \sqrt{\frac{E}{\nu} (1 - (\xi_{3} - (\xi_{3} - \xi_{2}) sn^{2} [\kappa T_{1}, \zeta]))}, & \text{if } \sigma > 0 \\ \sqrt{\frac{E}{\nu} (1 - (\xi_{3} - (\xi_{3} - \xi_{2}) cn^{2} [\kappa T_{1}, \zeta]))}, & \text{if } \sigma \leq 0 \end{cases},$$

$$(44a)$$

$$a_2 = \begin{cases} \sqrt{E(\xi_3 - (\xi_3 - \xi_2)sn^2[\kappa T_1, \zeta])}, & \text{if } \sigma > 0\\ \sqrt{E(\xi_3 - (\xi_3 - \xi_2)cn^2[\kappa T_1, \zeta])}, & \text{if } \sigma \le 0 \end{cases}$$
 (44b)

Having obtained the analytical expressions for a_1 and a_2 , we can get the nonlinear frequency of the system as follows. Using Eq. (33), $\cos \gamma$ can be removed from Eqs. (30) and (32) to get

$$D_1 \beta_1 = \frac{a_2^2}{a_1} \Gamma_1 \sqrt{1 - \left(\frac{D_1 a_2}{a_1 a_2 \Gamma_2}\right)^2}, \tag{45a}$$

$$D_1 \beta_2 = a_1 \Gamma_2 \sqrt{1 - \left(\frac{D_1 a_2}{a_1 a_2 \Gamma_2}\right)^2}.$$
 (45b)

Accordingly, the nonlinear frequencies of the system can be obtained as

$$\omega_{nl1} = \omega_1 + \epsilon D_1 \beta_1, \omega_{nl2} = \omega_2 + \epsilon D_1 \beta_2.$$

By substituting Eqs. (44) and (45) back in Eq. (17), we get the analytical expression for y(t) and $\theta(t)$. Detailed results from these amplitude expressions are presented in the next section.

Results and Discussion

In this section, numerical simulations are considered to examine the free vibrations of the UPM machine with nonlinear isolators. The numerical simulations are based on the parameters listed in Table 1.

TABLE 1: Key parameters of UPM machine used in the simulations.

Value	Units
1182	(kg)
96	$(kg-m^2)$
880	(kN/m)
1200	(kN/m)
100	(kN/m^2)
400	(kN/m^2)
295	(mm)
	1182 96 880 1200 100 400

The first part of the analysis is to validate the obtained closed form expressions and determine the value of ϵ (depends on the system parameters) that validates our assumption of weakly nonlinear system. The comparison between the numerical simulations from Eq. (4) and results from MMS (Eqs. (44) and (45)) are presented for $\epsilon = 0.1$, $\epsilon = 0.01$ and $\epsilon = 0.001$ with initial conditions y(0) = 1, $\dot{y}(0) = 0$, $\theta(0) = 1$, $\dot{\theta}(0) = 0$. The initial conditions for a_1 and a_2 can be obtained accordingly using Eqs. (17) and (28). Note that the employed initial conditions can excite both modes and further cause the existence of quasiperiodic solutions in the system. For the numerical simulation of Eq. (4), we have used the built-in command 'ode45' in Matlab with very tight absolute tolerance and relative tolerance $(1e^{-10})$.

Also, we emphasize that we have used numerical integration technique to get β_1 and β_2 as it is difficult to get the analytical expressions for β_1 and β_2 due to the appearance of Jacobi elliptic function. From Fig. 4 we can observe that there is an excellent agreement between the numerical simulations and analytical solutions for all values of ϵ . This agreement further improves by reducing the value of epsilon. For instance, there is almost perfect match with $\epsilon=0.001$. Since we are considering the initial conditions corresponding to the complex solutions in the system for comparison, the value of $\epsilon=0.001$ will be valid for the other initial conditions too. Therefore, in the remainder of this work, we have chosen $\epsilon=0.001$ for the analysis.

After deciding the value of ϵ , we present the effect of isolator location on ν , which is proportional to the initial energy of the system. On plotting ν for the different values of h, we can observe that ν always remains positive as there are no regenerative elements present in the system [25]. Note that the value of ν decreases to zero as h approaches zero (as shown in the inset of Fig. 5a), which is further evident from the fact that contribution of one mode to another decreases as h decreases due to mode coupling through h (Eq. (2)). Also, the peak value of ν (ν_{max} =2.418) at h = 0 represents discontinuous point because there is no coupling between the modes and it

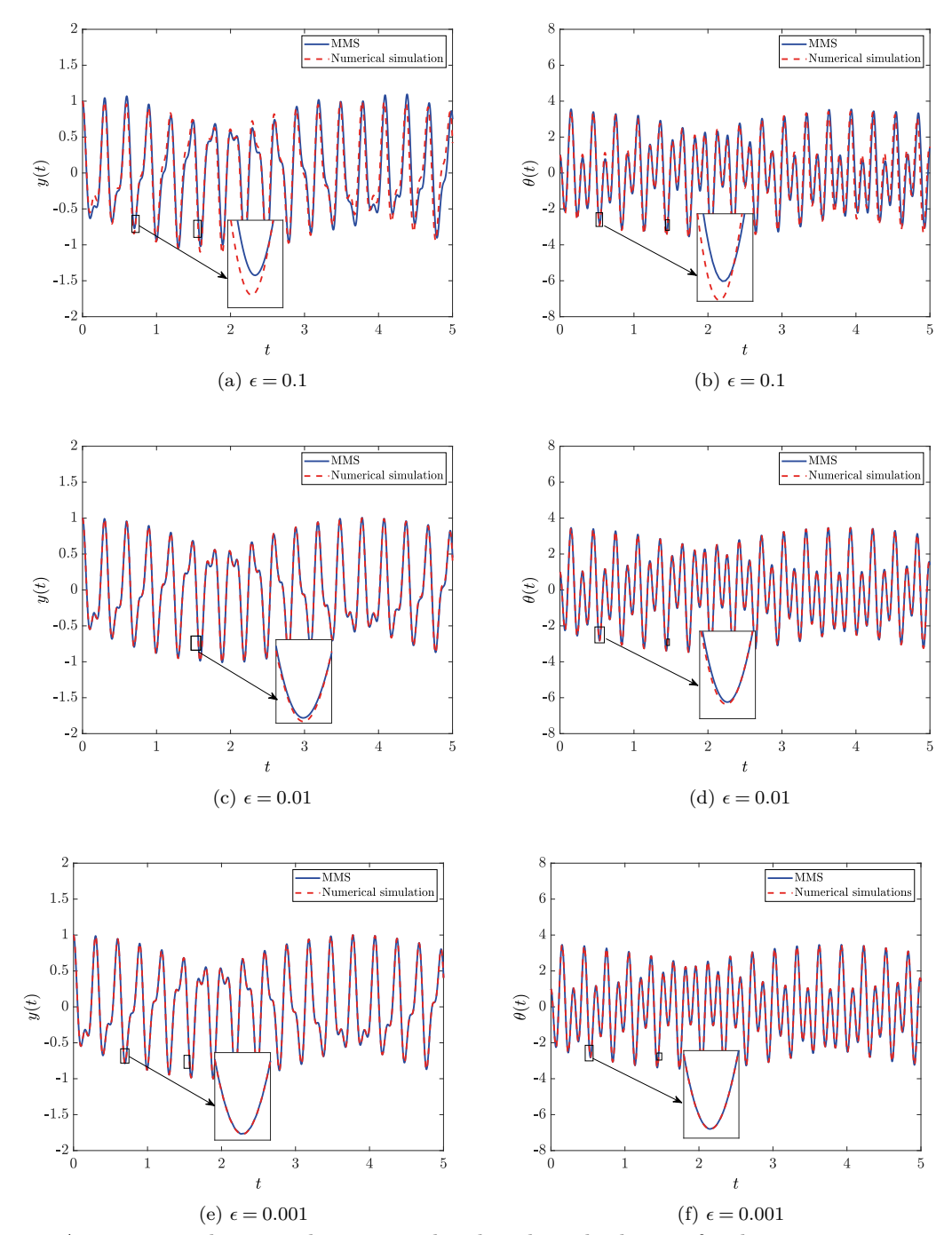


FIGURE 4: A comparison between the numerical and analytical solutions for the given system parameters in Table 1 (a), (c), (e) transnational motion, y(t) and (b), (d), (f) rotational motion, $\theta(t)$ with different values of ϵ ($\epsilon = 0.1$, 0.01 and 0.001) and h = -0.2 m.

becomes the ratio of higher natural frequency to lower nature frequency (Eq. (34), (35)). To further explore the effect of ν on the modal amplitudes a_1 and a_2 , we consider two different values of h viz. h=-0.2 m and h=0 m corresponding to finite and maximum values of ν , respectively and the results are shown in Fig. 5. The energy exchange between the two modal amplitudes can be clearly observed in Fig. 5d. It can be observed that the modal energy exchange significantly depends on the

location of the isolators, h. Now, we explore the effect of isolator location on the detuning parameter and accordingly on the modal amplitudes. Fig. 6 depicts the relationship between h and the value of detuning parameter ($\sigma\epsilon$). From this figure, it can be observed that the variation of the detuning parameter is symmetric about h=0 and attains a minimum value at h=0. Also, for the given values of system parameters in Table 1, the detuning parameter changes sign i.e., it becomes zero at

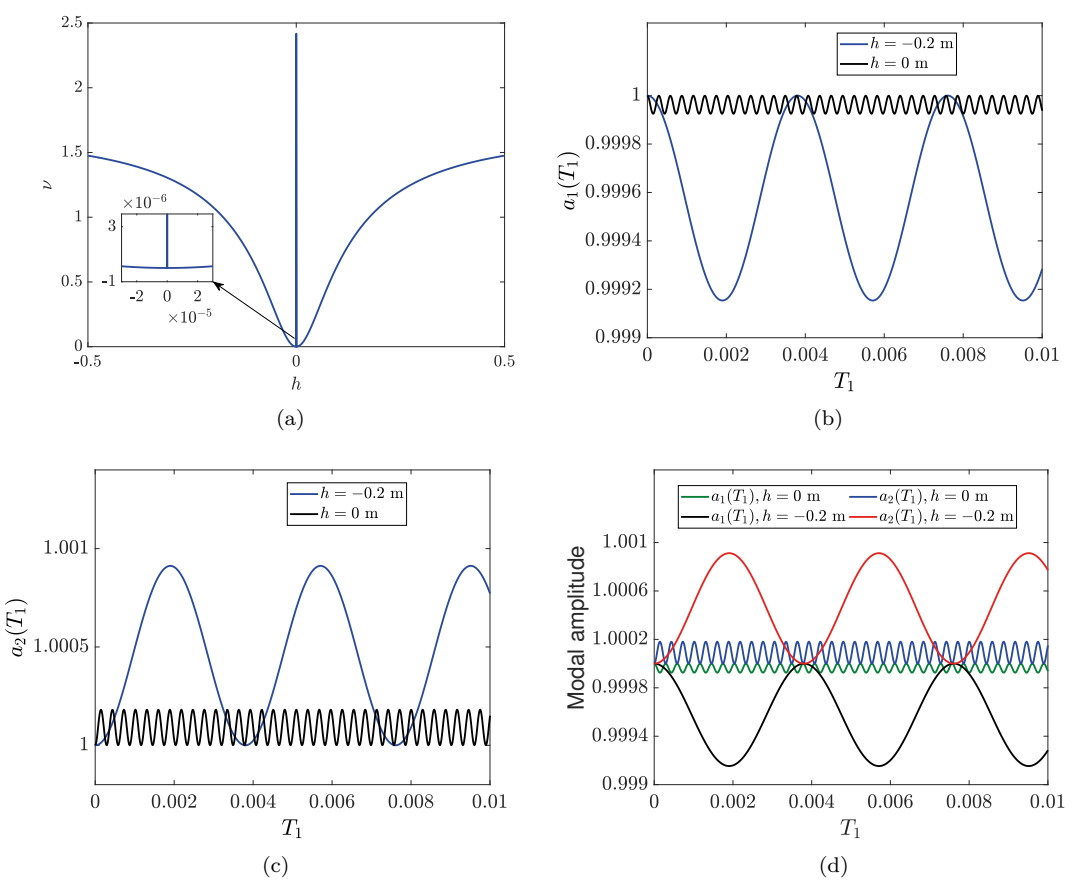


FIGURE 5: (a) Variation of ν with h. Slow time variation of the modal amplitudes (b) $a_1(T_1)$, (c) $a_2(T_1)$, and (d) the energy exchange between two modes, for h = -0.2 m, and h = 0 m with initial conditions $a_1(0) = 1$ and $a_2(0) = 1$.

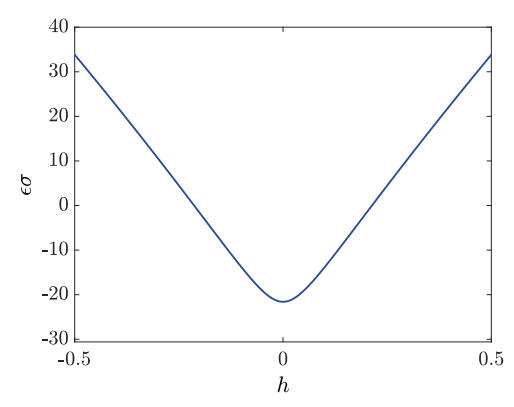


FIGURE 6: Variation of the detuning parameter with h for the given system parameters.

 $h=\pm 0.2134$ m. This situation further represents the case of internal resonance between the two modes $(\omega_1=2\omega_2)$. Note that the positive and negative values of h represent the location of isolator above and below the center of gravity of UPM, respectively. To further explore the effect of detuning parameter, via the height of isolator, on the system dynamics we choose two values of h corresponding to negative and positive values of detuning parameter for numerical simulation. In particular, we have chosen $h=\pm 0.116$ m, as the optimum value of h reported in the earlier work is h=-0.116 m [13]. Fig-

ure 7 shows the slow time variation of modal amplitudes, a_1 and a_2 for $h=\pm 0.116$ m. From this figure, it can be observed that placing the isolators below the center of gravity of UPM has more adverse effect on modal amplitudes as compared to placement of isolators above the center of gravity. This observation is contrary to the results shown for the linear vibration of the UPM [13]. On further exploring the dynamics of system for different values of h, we observe that amplitude of a_1 and a_2 increase as the value of h approaches towards h=0.2134 m (corresponding to internal resonance) and largest vibrations occur at h=0.2134 m (see Figs. 8a and b) due to internal resonance between the two modes. This observations are in consistency with negative values of h too (Figs 8 c and d).

Conclusion

We studied the nonlinear vibration of a UPM machine analytically using the method of multiple scales. Based on the experimental results, we assumed the stiffness of the pneumatic isolators to be a combination of linear and quadratic stiffnesses. In our mathematical formulation, the horizontal and torsional motions were also linearly and nonlinearly coupled through the location of the vibration isolators, h. The closed form solution for the

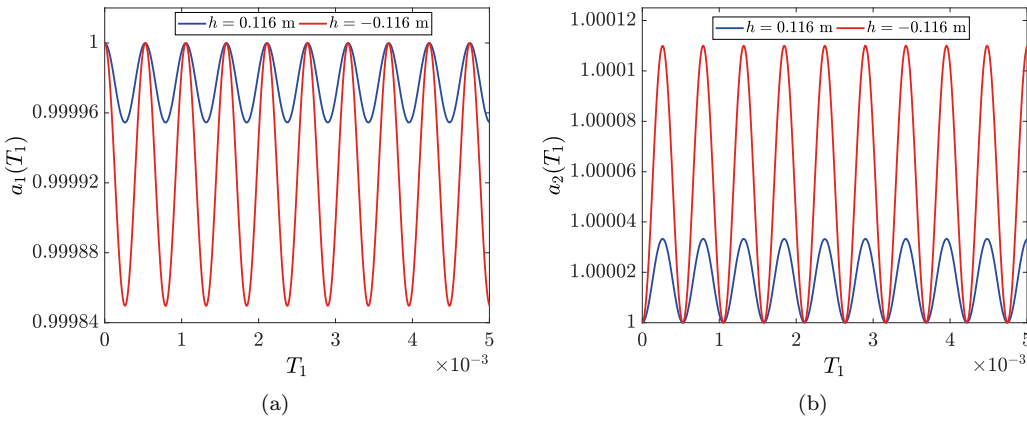


FIGURE 7: Slow time variation of the modal amplitudes (a) a_1 and (b) a_2 for $h = \pm 0.116$ and initial conditions $a_1(0) = 1$ and $a_2(0) = 1$.

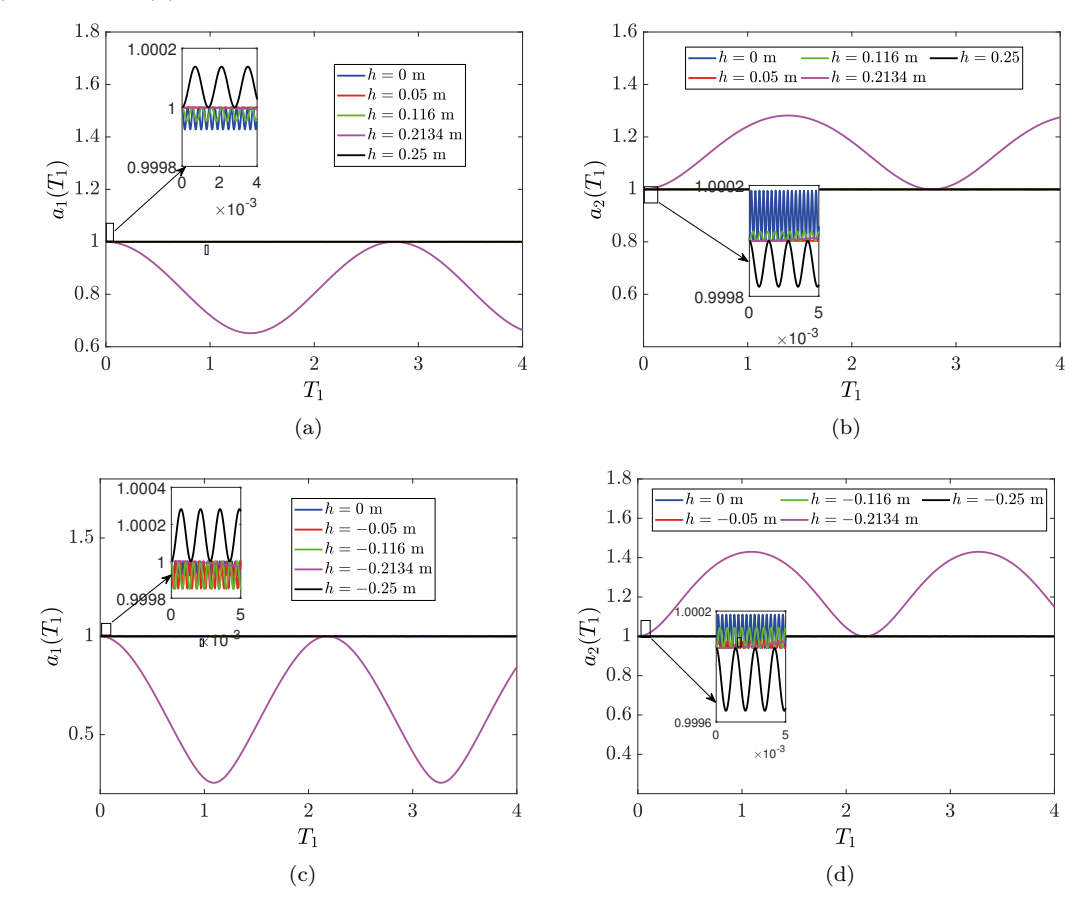


FIGURE 8: Slow time variation of the modal amplitudes (a) a_1 and (b) a_2 for different values of h and initial conditions $a_1(0) = 1$ and $a_2(0) = 1$.

modal amplitudes, corresponding to the nearly resonant case, was obtained using MMS and expressed in terms of Jacobi elliptic functions. The obtained analytical expressions were validated using direct numerical simulations and the results showed very good agreement. Numerical simulations further suggested that small amplitude oscillations occur at the value of h close to zero. Moreover, the vibration amplitude increased as h approached the location of the internal resonance ($h=0.2134~\mathrm{m}$). Also, it was observed that placing isolator below the level of center

of gravity is less effective as compared to the placement of isolator above the level of centre of gravity of UPM. Furthermore, it was also demonstrated that modal energy exchange is significantly dependent on the location of the pneumatic isolators relative to the center of gravity of the UPM machine. Overall, the findings in this paper contradict recent studies of passively-isolated systems and suggest that nonlinear mode coupling can yield worst vibration isolation, especially, when the location of the vibration isolators corresponds to the internal reso-

nance case. In our future work, we will extend this work by including damping and forcing terms and analyze the isolated system under sub-harmonic and super-harmonic resonances. We will also determine the optimum h for which superior vibration isolation can be achieved.

ACKNOWLEDGMENT

This work is funded by National Science Foundation (NSF) Award CMMI #2000984: Nonlinear Dynamics of Pneumatic Isolators in Ultra-Precising Manufacturing Machine.

REFERENCES

- Alting, L., Kimura, F., Hansen, H. N., and Bissacco, G., 2003. "Micro engineering". CIRP Annals-Manufacturing Technology, 52(2), pp. 635–657.
- [2] Hansen, H. N., Carneiro, K., Haitjema, H., and De Chiffre, L., 2006. "Dimensional micro and nano metrology". CIRP annals, 55(2), pp. 721–743.
- [3] Ehmann, K. F., 2007. "A synopsis of us micromanufacturing research and development activities and trends". *Borovets, Bulgaria*, pp. 7–13.
- [4] Karnopp, D., 1995. "Active and semi-active vibration isolation". In Current Advances in Mechanical Design and Production VI. Elsevier, pp. 409–423.
- [5] Schellekens, P., Rosielle, N., Vermeulen, H., Vermeulen, M. M. P. A., Wetzels, S. F. C. L., and Pril, W., 1998. "Design for precision: current status and trends". *Cirp Annals*, 47(2), pp. 557–586.
- [6] Liu, Y., Waters, T. P., and Brennan, M. J., 2005. "A comparison of semi-active damping control strategies for vibration isolation of harmonic disturbances". *Journal of Sound and Vibration*, 280(1-2), pp. 21–39.
- [7] DeBra, D. B., 1992. "Vibration isolation of precision machine tools and instruments". CIRP Annals-Manufacturing Technology, 41(2), pp. 711–718.
- [8] Rivin, E. I., 1995. "Vibration isolation of precision equipment". *Precision Engineering*, 17(1), pp. 41–56.
- [9] Franchek, M. A., Ryan, M. W., and Bernhard, R. J., 1996. "Adaptive passive vibration control". *Journal* of Sound and Vibration, 189(5), pp. 565–585.
- [10] Ryaboy, V. M., 2014. "Static and dynamic stability of pneumatic vibration isolators and systems of isolators". *Journal of sound and vibration*, 333(1), pp. 31–51.
- [11] Subrahmanyan, P. K., and Trumper, D. L., 2000. "Synthesis of passive vibration isolation mounts for machine tools-a control systems paradigm". In American Control Conference, 2000. Proceedings of the 2000, Vol. 4, IEEE, pp. 2886–2891.
- [12] Rivin, E. I., 2006. "Vibration isolation of precision objects". Sound and Vibration, 40(7), pp. 12–20.
- [13] Okwudire, C. E., 2012. "A study on the effects

- of isolator, motor and work surface heights on the vibrations of ultra-precision machine tools". *Proc ICOMM, Evanston, Illinois, March*, pp. 31–36.
- [14] Shin, Y.-H., Kim, K.-J., Chang, P.-H., and Han, D. K., 2010. "Three degrees of freedom active control of pneumatic vibration isolation table by pneumatic and time delay control technique". *Journal of Vibration and Acoustics*, 132(5), p. 051013.
- [15] Vermeulen, M. M. P. A., Rosielle, P. C. J. N., and Schellekens, P. H. J., 1998. "Design of a high-precision 3d-coordinate measuring machine". *CIRP Annals-Manufacturing Technology*, 47(1), pp. 447–450.
- [16] Kato, T., Kawashima, K., Sawamoto, K., and Kagawa, T., 2007. "Active control of a pneumatic isolation table using model following control and a pressure differentiator". Precision Engineering, 31(3), pp. 269–275.
- [17] Erin, C., Wilson, B., and Zapfe, J., 1998. "An improved model of a pneumatic vibration isolator: theory and experiment". *Journal of sound and vibration*, 218(1), pp. 81–101.
- [18] Bukhari, M., and Barry, O., 2017. "On the nonlinear vibration analysis of ultra precision manufacturing machines with mode coupling". In ASME 2017 International Design Engineering Technical Conferences and Computers and Information in Engineering Conference.
- [19] Ewins, D. J., Rao, S. S., and Braun, S. G., 2002. Encyclopedia of Vibration, Three-Volume Set. Academic press.
- [20] Racca Sr, R., 1982. "How to select power-train isolators for good performance and long service life". SAE Transactions, pp. 3439–3450.
- [21] Andrews, F., 2012. Items which can compromise vibration isolation.
- [22] Okwudire, C. E., and Lee, J., 2013. "Minimization of the residual vibrations of ultra-precision manufacturing machines via optimal placement of vibration isolators". *Precision Engineering*, 37(2), pp. 425–432.
- [23] Heertjes, M., and van de Wouw, N., 2006. "Non-linear dynamics and control of a pneumatic vibration isolator". *Journal of Vibration and acoustics*, 128(4), pp. 439–448.
- [24] Balachandran, B., and Nayfeh, A. H., 1992. "Cyclic motions near a hopf bifurcation of a four-dimensional system". *Nonlinear Dynamics*, 3(1), pp. 19–39.
- [25] Nayfeh, A. H., and Mook, D. T., 2008. Nonlinear oscillations. John Wiley & Sons.